Effect of packing fraction on granular jetting from solid sphere entry into aerated and fluidized beds

J. O. Marston,[1] J. P. K. Seville,[1] Y-V. Cheun,[1] A. Ingram,[1]
S. P. Decent,[2] and M. J. H. Simmons[1]
[1]*Department of Chemical Engineering, University of Birmingham, Edgbaston, Birmingham, B15 2TT United Kingdom*
[2]*School of Mathematics, University of Birmingham, Edgbaston, Birmingham, B15 2TT United Kingdom*

(Received 1 August 2007; accepted 11 December 2007; published online 19 February 2008)

When a solid sphere impacts on a granular bed, a high-speed vertical jet can arise following the collapse of the cavity that is formed by the penetration of the sphere into the bed. The jet then becomes unstable and breaks into discrete clusters due to density inhomogeneities. In this study, the jetting process was observed using high-speed photography and determined to be a function not only of impact velocity and particle size, but also of the packing fraction in the bed during the impact. Experiments were performed for two different bed diameters, two bed heights, and two impact velocities. Under certain conditions, below a threshold packing fraction, the jet is seen to divide into two distinct parts: a thin upper section followed by a thick base. Geometrical constraints are also shown to be critical in determining the dynamics of the jet. © *2008 American Institute of Physics*. [DOI: 10.1063/1.2835008]

I. INTRODUCTION

Jetting following the impact of liquid drops and solid spheres onto liquid surfaces is a well documented phenomenon that has received significant experimental and theoretical examination to elucidate the underlying physics and governing parameters (see Yarin[1] for a review).

Thoroddsen and Shen[2] performed the first experiments for the granular equivalent of the liquid case by dropping solid spheres onto a deep bed of loose granular material. The bed was sufficiently loose, i.e., low solid packing fraction, that the sphere penetrated the bed and left a cylindrical cavity below the surface. This cavity collapsed, resulting in the formation of a granular jet, which was seen to rise above the surface. The jet height was found to increase with impact velocity and decreasing grain size of the bed. In these experiments, the bed was not characterized in terms of the packing fraction.

Since this remarkable study, the granular jetting phenomenon has been reproduced by several authors (Lohse *et al.*,[3] Hou *et al.*,[4,5] Royer *et al.*,[6] and Bulychev *et al.*[7]). Lohse *et al.*[3] performed similar experiments for a finer particle size (average 40 μm) where the bed was first "decompactified" by aeration through a bottom plate, yielding an initial packing fraction (volume fraction of solid) of 0.41. For this initial bed state, the height of the resulting jet was always found to exceed the initial release height of the impacting sphere, in contrast to the experiments of Thoroddsen and Shen.[2] Lohse *et al.*[3] also performed a pseudo two-dimensional (2D) experiment and numerical simulations, which showed that the cavity collapse results in a jet that travels vertically downwards (following the sphere) as well as the jet that rises above the surface. A model of cavity collapse is presented that gives a collapse ("pinch-off") depth $z_c \approx RFr^{1/3}$, where R is the sphere radius and $Fr = U_i^2/(gR)$ is the Froude number, where U_i is the impact velocity and g is the acceleration due to gravity.

Royer *et al.*[6] applied x-ray radiography to study the formation of the jet under various external pressures. They found the maximum jet height to be strongly dependent on the surrounding air pressure, which was varied by placing the equipment in a vacuum chamber. In their experiments, the bed (comprised of 50 μm spherical glass beads) was prepared by aeration with dry nitrogen, which was turned off prior to impact, leaving a packing fraction of 0.55. Not only was the jet height found to be strongly dependent on the ambient gas pressure, but the jet itself was observed to take on a two-stage structure: for ambient pressures below 5.3 kPa, only a thin jet is observed (similar to that seen by Thoroddsen and Shen and Lohse *et al.*); above this threshold pressure, a two-stage structure emerges with a thick base following a thin top jet. On further increasing the ambient gas pressure, the thin jet is completely suppressed and only a thick jet is observed. Visualization of the cavity collapse inside the vessel showed a secondary cavity pinch-off. The authors, therefore, concluded that it is the compression of the trapped air pocket pushing material up that results in the formation of the thick jet. This is discussed later in more detail.

Experiments by Hou *et al.*[4,5] used a particle size range of 74–100 μm with an initial packing fraction of 0.54, and they observed jetting following the impact of a sphere on the bed, although the post-impact jetting was not the primary focus of this study.

Bulychev *et al.*[7] used a similar experimental arrangement to that of Royer *et al.*[6] to study the effect of ambient gas pressure on the jetting phenomenon using various projectile shapes. In these experiments, various particle size ranges were used as the target medium, but the bed was not

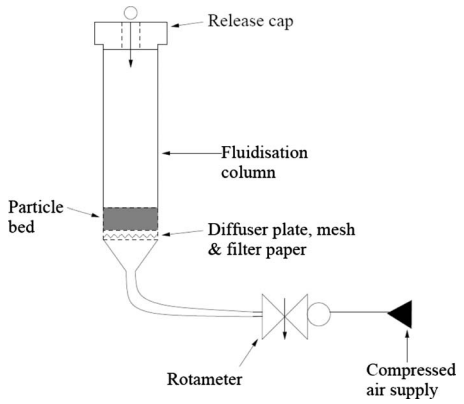

FIG. 1. Schematic of the experimental setup. Not to scale.

characterized and no measurements of the jet height or structure were reported.

All of these studies mention that the preparation of the bed and the level of compaction have a significant influence on the jetting behavior, and, in fact, Lohse *et al.*[3] achieved their initial bed states by fluidization. However, none have considered the influence of keeping a constant and uniform gas velocity through the granular bed during impact to vary the packing fraction while keeping other parameters constant.

In the present study, experiments were performed to examine the effect of keeping a constant level of aeration during the impact of a solid sphere onto a granular bed. Geldart Group A particles (Geldart[8]) were used in the bed for their ability to expand in a stable manner between the minimum fluidization velocity, U_{mf}, and the minimum bubbling velocity, U_{mb}. As such, by controlling the gas velocity, U_g, between these limits, the bed density and packing fraction can be varied.

The preparation of the bed involved first fluidizing the bed (above U_{mb}), then reducing U_g to the required level, which was generally below the minimum bubbling velocity, U_{mb}. When the bed is compacted (i.e., no prior aeration), no jetting occurs. If the initial bed packing is below a threshold value, jetting occurs with the appearance of one or two discrete sections. The maximum height of the jet was measured directly as a function of release height (impact velocity), ball diameter, particle size, and gas velocity (packing fraction) in two different geometries. Under certain conditions, the jet has two distinct parts, as seen by Royer *et al.*[6]

II. MATERIALS AND METHODS

A schematic of the experimental setup used for these experiments is shown in Fig. 1. The main component is a glass fluidization column. The bed of particles sits in the column above a gas distribution system, consisting of a metallic distributor plate, a fine wire mesh, and layers of filter paper, ensuring a uniform gas flow across the bed.

Two different sizes of fluidization columns were used in these experiments, one small with an inner diameter of 7 cm and one large with an inner diameter 15 cm. When poured, the initial bed heights, h_b, were 7 and 10 cm, respectively.

TABLE I. Conditions for the majority of experiments performed in this study. Some experiments were also performed with a larger ball (D=40 mm) in both vessels.

Vessel inner diameter (cm)	7	15
Release height, h_r (cm)	33	90
Bed height, h_b (cm)	7	10
Bead diameter, d_b (μm)	65,78	65,78
Ball diameter, D (mm)	10,20	10,20

Glass beads (Sigmund Lindner GmbH) with nominal diameters d_b=40–70 and 70–110 μm as stated by the manufacturer were used in both vessels.

Particle size analysis, performed on a Malvern wet particle sizer, shows that the mean particle diameters were 65 and 78 μm, respectively, with d_{10}=54 μm and d_{90}=80 μm for the former and d_{10}=62 μm and d_{90}=102 μm for the latter. For convenience, the mean particle sizes are quoted for the rest of this paper.

The significance of the size distribution of the particles is discussed later. The particles have a density of 2500 kgm^{-3}; the bulk density varies according to the packing, as seen later.

Two sphere sizes, D=10 and 20 mm, were used for the majority of the experiments. Caps with release tubes were fitted to the tops of the vessels to ensure centering and constant release height, h_r=33 and 90 cm, respectively, with resulting impact velocities U_i=2.5±0.1 and 4.2±0.1 ms^{-1}, however this was not the primary focus of this study. The conditions for the majority of the experiments are summarized in Table I, although a limited number of experiments were also performed for a larger sphere (D=40 mm) in both vessels (to investigate the effect of geometry).

To ensure consistency in preparation of the bed prior to impact, the beds were fluidized with dry air by first increasing the inlet air velocity to above U_{mb}, then gradually reducing to the required level. The bed height was measured at each set gas velocity in order to calculate a packing fraction. The experiments were performed mostly at aeration levels below U_{mb}. The packing fraction ϕ in the bed was in the range $0.49 \leq \phi \leq 0.62$ and was determined as a function of the superficial gas velocity, as shown in Fig. 2. Once the air flow through the bed exceeds U_{mb}, estimating the packing fraction and hence characterization of the bed becomes difficult. As such, the lower bound of the packing fraction was determined by U_{mb}. Expansion of the bed at gas velocities between U_{mf} and U_{mb} was typical of Geldart group A particles; under these conditions, the weight of the particles in the bed is exactly balanced by the air flow, yielding a linear relationship between pressure drop in the bed and depth so that the resulting packing fraction in the bed is uniform.[8,9]

To record the impact and subsequent jetting, a Photron APX monochrome high-speed camera (Photron Ltd, UK) was used at a recording rate of 3000 fps yielding a resolution of 512×1024 pixels and recording times of approximately 6 s, sufficient to observe the entire impact and post-impact events. Images are stored continuously onto the camera memory bank until stopped by an external manual trigger.

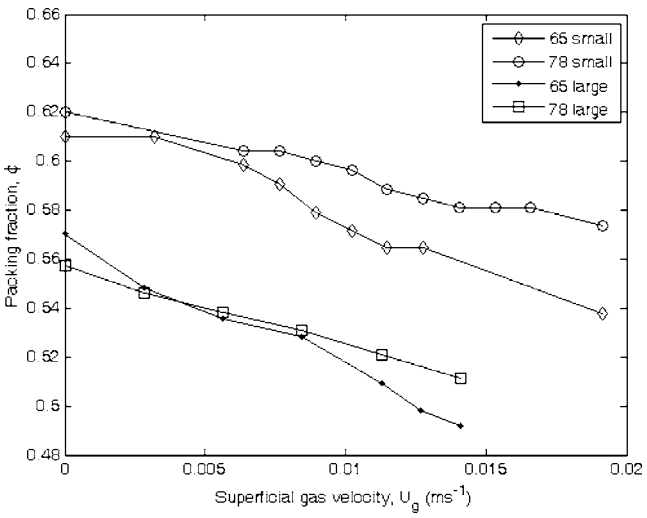

FIG. 2. Plot showing the packing fraction as a function of inlet (superficial) gas velocity. The legend indicates the particle diameter (μm) and vessel size (small, I.D.=7 cm; large, I.D.=15 cm).

The impact velocity of the spheres and the maximum jet height, $h_{j,\max}$, were measured directly from the recordings. Each individual experiment was repeated a minimum of three times to ensure reproducibility. The main purpose of this study is to show the reproducible qualitative and quantitative features of the jetting process as a function of the packing in the target bed—a parameter that has not been previously considered. In addition, we show that geometrical constraints are also important.

III. RESULTS AND DISCUSSION

Figure 3 shows the sequence of events for the impact of a 10 mm sphere onto a 10 cm deep bed (large vessel) of 78 μm glass beads from a release height of 90 cm. The bed was prepared as described above, yielding a packing fraction ϕ=0.56. The selected frames show the main features of the jetting process, similar to that previously reported (Thoroddsen and Shen,[2] Lohse *et al.*,[3] Hou *et al.*,[4,5] and Royer *et al.*[6]). The corona splash following impact (image c) is similar to that seen in liquid drop impact onto liquid sur-

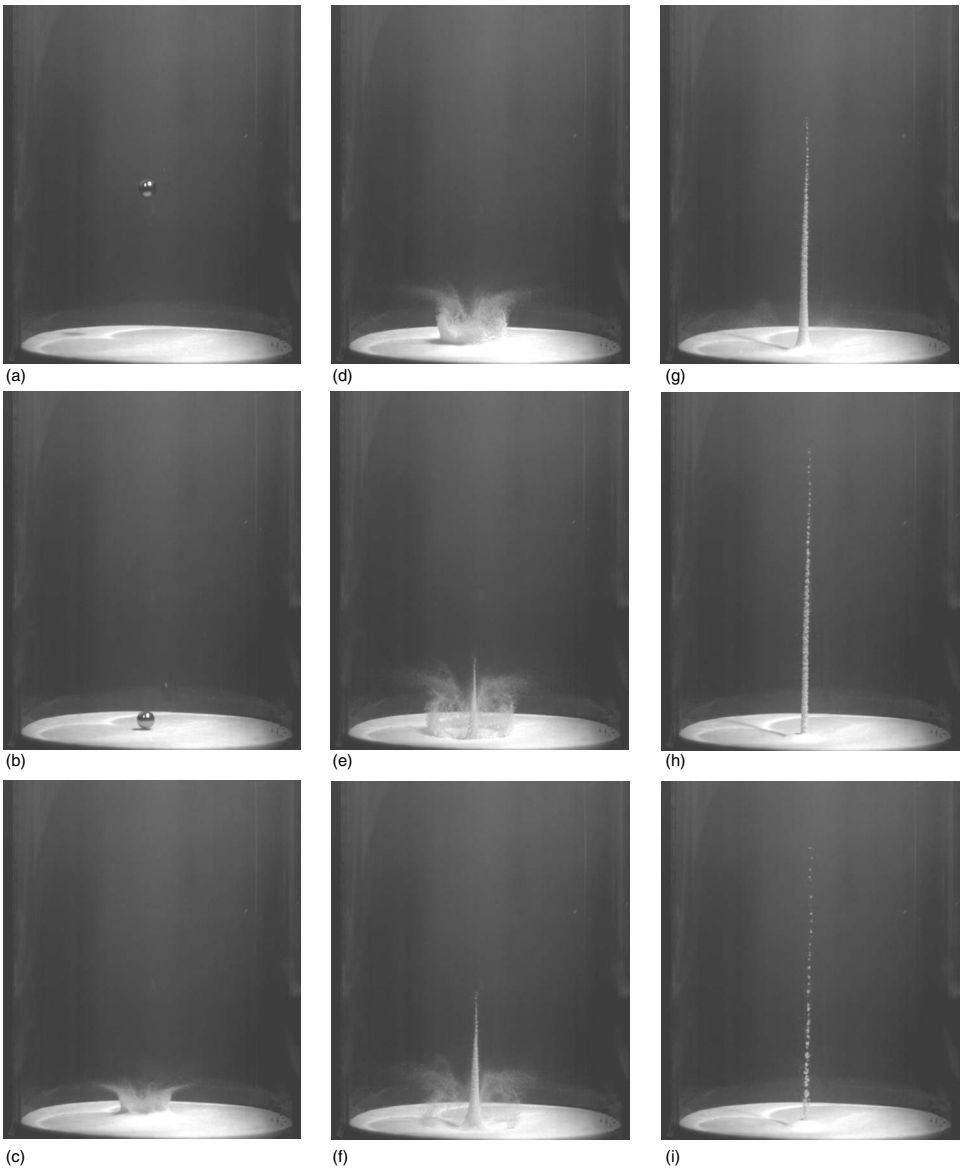

FIG. 3. Sequence of events for impact of a 10 mm sphere onto a 10 cm deep bed (large vessel, I.D.=15 cm) of 78 μm particles from a release height of 90 cm. There was no aeration during impact for these images, yielding a packing fraction, ϕ=0.56. Times from impact are −20, 0, 20, 50, 80, 100, 150, 200, and 300 ms. The maximum jet height in this instance is 16.5 cm.

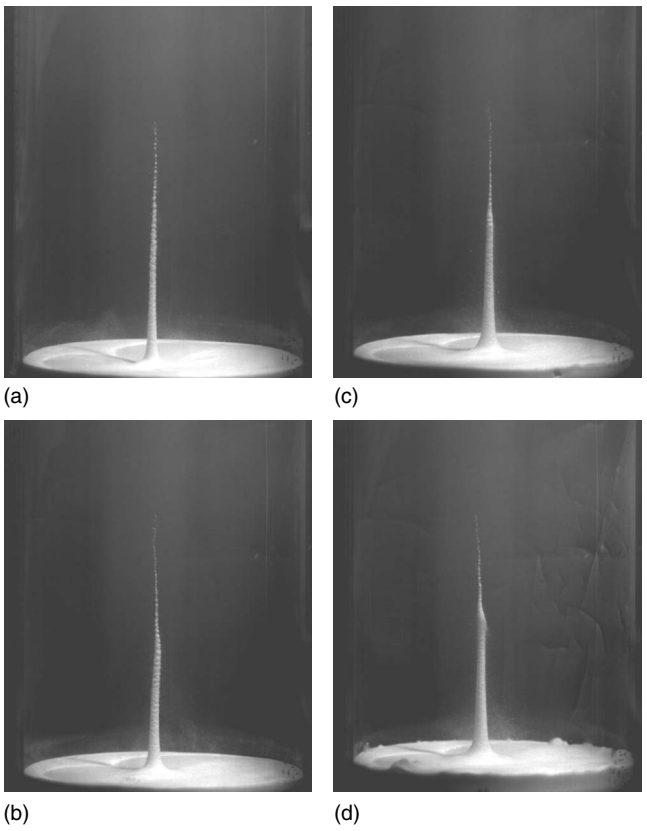

FIG. 4. Comparison of post-impact jetting under various bed packing conditions for a 10 mm sphere impacting a 10 cm deep bed of 78 μm particles. All images are taken at 150 ms after impact. The packing fractions were (a) ϕ=0.56, (b) ϕ=0.53, (c) ϕ=0.52, and (d) ϕ=0.51. Note that the jet height in each instance is comparable, but the jet begins to divide into two distinct parts as the packing fraction decreases.

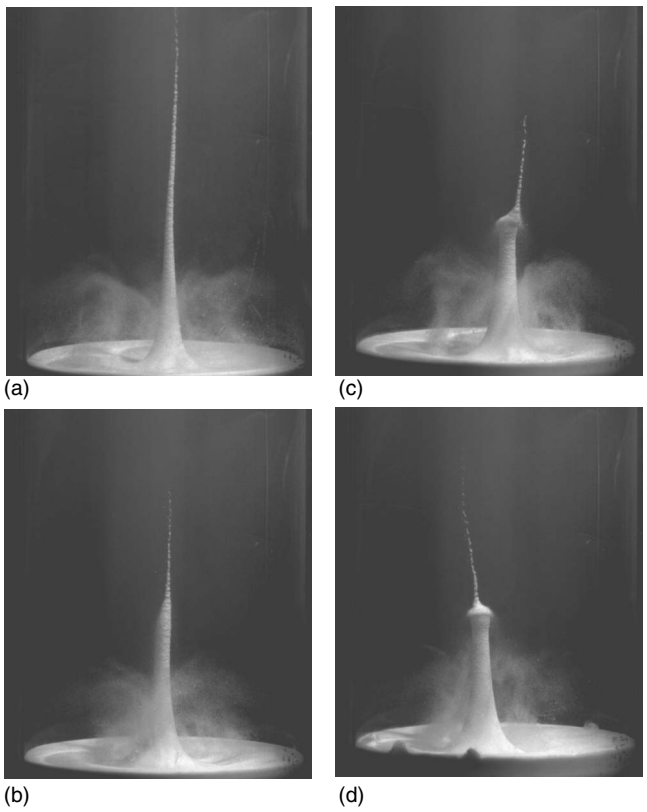

FIG. 5. Comparison of post-impact jetting under various bed packing conditions for a 20 mm sphere impacting a 10 cm deep bed of 78 μm particles. All images are taken at 150 ms after impact. The packing fractions were (a) ϕ=0.56, (b) ϕ=0.53, (c) ϕ=0.52, and (d) ϕ=0.51.

faces (Yarin[1]). This initial ejection of material is subject to the pressure reduction behind the falling sphere, and the resulting air flow can cause a slight collapse of the corona as seen in image (d); this is more easily seen for finer particle sizes, as discussed later (Fig. 8). The cavity formed by the penetration of the sphere collapses at a depth z_c (i.e., the "pinch-off" depth) beneath the surface and results in the emergence of the vertical jet above the surface of the bed seen in image (e). This jet rises to a maximum of 16.5 cm while undergoing a clustering instability (Möbius[10]), then falls back to the surface of the bed at the site of initial impact—seen in images (f)–(i). The entire process for this particular instance takes place in less than half a second.

The maximum jet height in Fig. 3 is consistent with the data in Thoroddsen and Shen[2] for the 80 μm particles, suggesting a similar initial state of the bed.

In Fig. 3, a single narrow jet above the surface is seen, which then conforms to the model of cavity collapse proposed by Lohse *et al.*[3] In contrast, Fig. 4 shows frames from experiments using the same parameters as Fig. 3 (large vessel, d_b=78 μm, D=10 mm), performed under various bed conditions in which the aeration was kept at a constant level during impact, yielding packing fractions ϕ=0.56, 0.53, 0.52, and 0.51, respectively. The images shown are single frames each taken from the video sequence at 150 ms after impact. As the packing fraction decreases, the jet is seen to divide into two distinct parts—this is most readily seen in image (d) for ϕ=0.51. The total height of the jet (thick and thin combined) increases marginally with decreasing packing fraction, although no quantifiable trend is established (discussed later). The height at which the jet appears to divide is also fairly constant—in the series of experiments shown, this division occurs at about 7 cm.

The distinction between a single narrow jet and a jet consisting of a thick and thin part has only been reported before by Royer *et al.*[6] As noted earlier, their experiments were carried out at varying gas pressures in the chamber, and the observation of a two-jet structure coincided with a reduction in pressure below a certain level. In the experiments reported here, the ambient (atmospheric) gas pressure remains constant and a compound jet occurs below a certain threshold packing fraction. The fact that we do not observe a thick part to the jet above certain packing fractions may be an indication that variations in the ambient pressure may have inadvertently altered the packing in the experiments by Royer *et al.*[6]

Figure 5 shows the equivalent image sets for the jetting process following the impact of a 20 mm sphere in the large vessel (h_r=90 cm, d_b=78 μm). Again, the images shown are single frames taken from the video recording 150 ms after impact. The packing fractions are the same as those used in Fig. 4, ϕ=0.56, 0.53, 0.52, and 0.51, respectively. Image (a), for the base case with no aeration during impact, shows a single narrow jet (extending out of the frame). The maximum

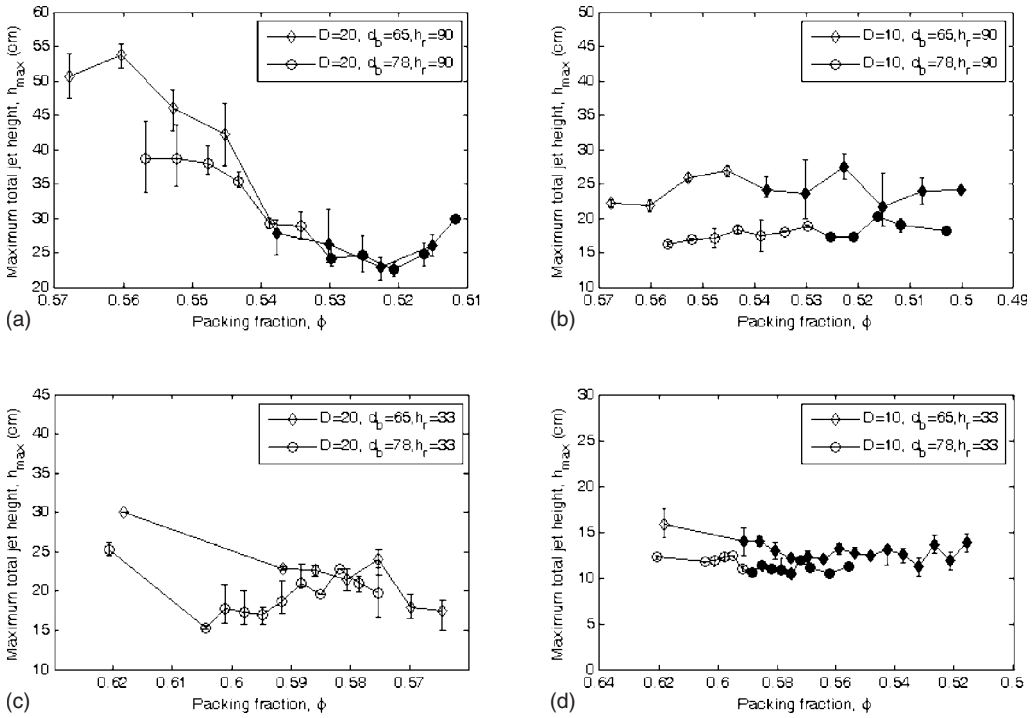

FIG. 6. Maximum jet heights plotted as a function of the bed packing fraction for (a) h_r=90 cm, D=20 mm; (b) h_r=90 cm, D=10 mm; (c) h_r=33 cm, D=20 mm; and (d) h_r=33 cm, D=10 mm. The error bars shown are generated from averaging repeat experiments. The filled data points indicate a jet with a two-stage structure.

height attained for this jet was 40.1 cm. The two-jet structure seen in images (b), (c), and (d) is now much more pronounced than for the 10 mm sphere, and in images (c) and (d), the thick jet has developed a distinct "shoulder" marking the division between the two parts of the jet. For these experiments, the maximum jet height decreases monotonically with ϕ until ϕ=0.52. A slight increase in jet height is observed at ϕ=0.51 and then a gradual decrease as the aeration level is brought to such a level that bubbles appear in the bed, at which point the thin jet is completely suppressed and only the thick jet is observed. For $\phi<0.51$ ($U_g>U_{mb}$), however, the jetting becomes irregular and not reproducible, hence these images are not shown.

Data for the maximum jet heights as a function of packing fraction for all the experimental conditions in Table I are shown in Figs. 6(a)–6(d). From the plots it is evident that there is scatter in the data for all experimental conditions, which may be due partly to the size distribution of the particles used. Taller jets are always obtained with the finer particles, in accordance with previous works. For the experiments performed in the large vessel with h_r=90 cm and D=20 mm in Fig. 6(a), the jet height becomes independent of the particle size for $\phi<0.54$ and the general trend observed is qualitatively similar for both particle sizes. In Figs. 6(b) and 6(d) for the smaller sphere, D=10 mm, there is a much weaker dependence on the packing fraction for both the large and small vessels and both particle sizes, suggesting that the dependence on the initial state of the bed is only a feature of the more constrained systems.

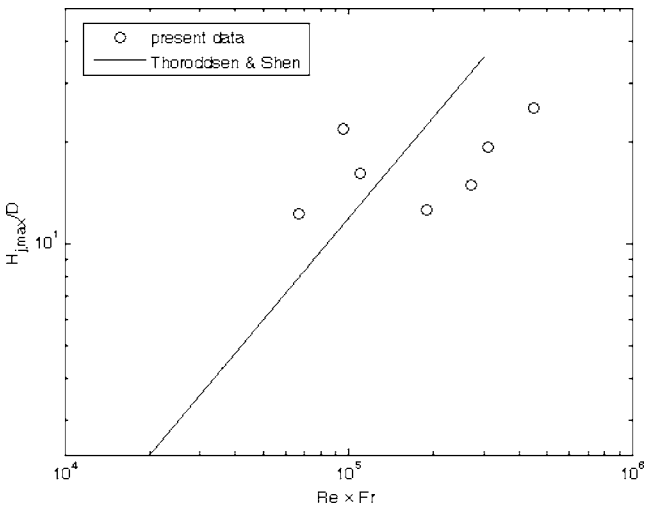

FIG. 7. Maximum jet heights normalized by the sphere diameter plotted against the product of the Reynolds and Froude number. The solid line is the empirical correlation deduced by Thoroddsen and Shen (Ref. 2).

TABLE II. Predicted pinch-off depth of the cavity for the experimental conditions used. $z_c \sim DFr^{1/3}$ is the scaling proposed by Lohse *et al.* (Ref. 3). For D=40 mm, the collapse is clearly obscured by the sphere itself since the sphere will have reached the bottom of the vessel before the cavity can pinch off.

Vessel inner diameter (cm)	7	7	7	15	15	15
Release height, h_r (cm)	33	33	33	90	90	90
Sphere diameter, D (mm)	10	20	40	10	20	40
Bed depth, h_b (cm)	7	7	7	10	10	10
Pinch-off depth, z_c (cm)	2.5	4	6.4	3.5	5.6	8.9

The maximum jet heights shown are the total jet heights (either for the single narrow jet or the combined height of the thick and thin jets), and the data for the beds with no aeration during impact have been compared to data obtained by Thoroddsen and Shen[2] in Fig. 7. This logarithmic plot shows the maximum jet height normalized by the sphere diameter against the product of the Reynolds $[\mathrm{Re}=1/2(D/d_b)^2]$ and Froude $[\mathrm{Fr}=U_i/(\sqrt{gD})]$ numbers. Clearly, the maximum jet height is still dependent on the same parameters as in the work by Thoroddsen and Shen, but the dependence is weaker.

It should also be noted here that the bed heights used were intentionally much shallower than in previous studies, and in more constricted geometries, in order to examine their possible influence, which has not been considered in previous analyses. Since it is clear that geometric constraints are

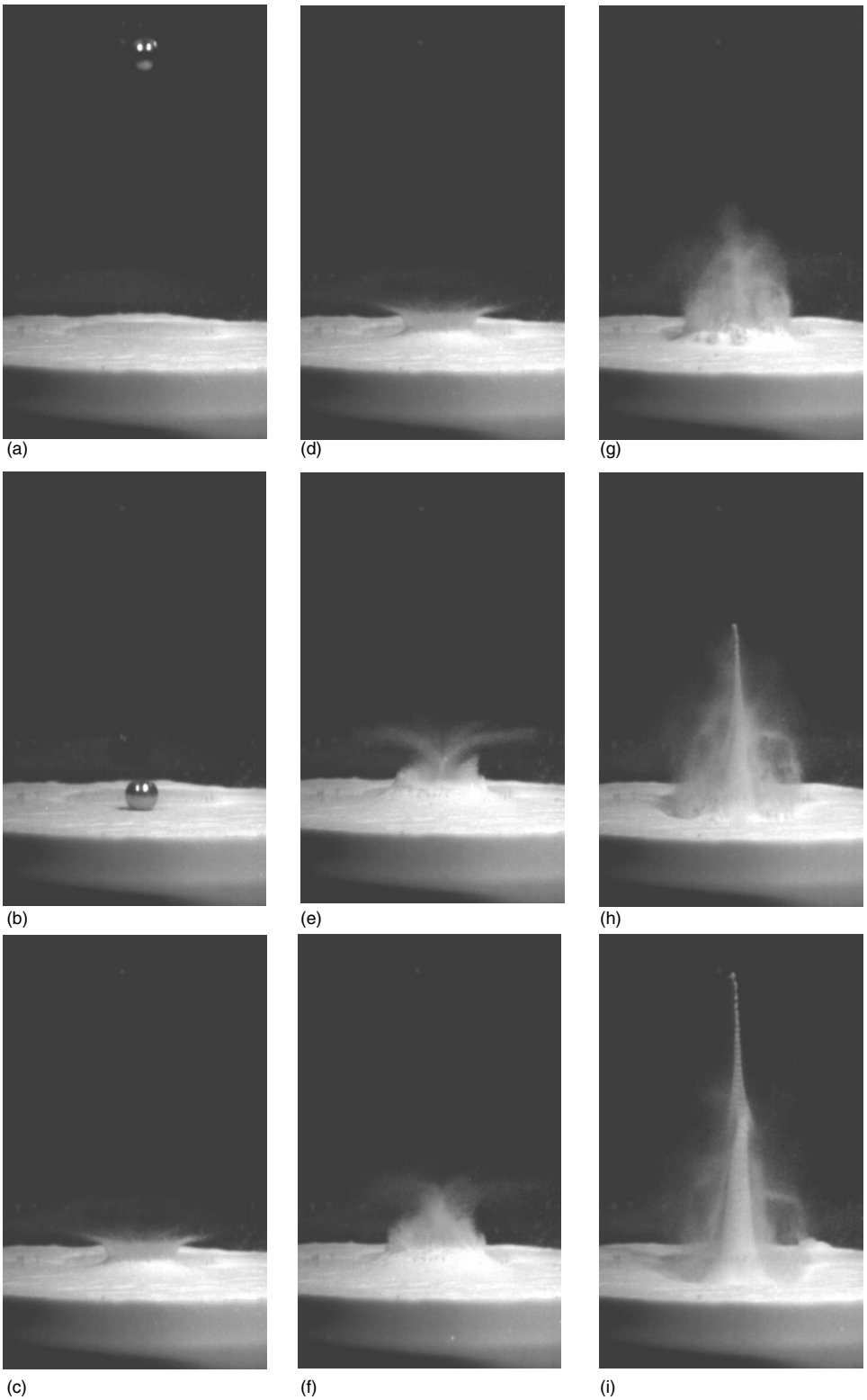

FIG. 8. Sequence of events for impact of a 10 mm sphere onto a 10 cm deep bed of 65 μm particles from a release height of 90 cm. The aeration was set to a constant level of 7 L/min during impact for these images, corresponding to $u_g=9.92\times10^{-3}\ \mathrm{ms}^{-1}$ and yielding a packing fraction, $\phi=0.52$. Times from impact are −20, 0, 10, 20, 30, 50, 70, 90, and 110 ms. The initial corona splash closes following the pressure reduction behind the falling sphere and distorts the rising jet.

important, some of the scatter must also be attributed to increased particle-wall interactions and the fact that the depth of collapse of the cavity is now comparable to the depth of the bed, according to the scalings by Lohse *et al.*[3] This model of inertial collapse predicts the cavity pinch-off depth $z_c \sim RFr^{1/3}$, where $\mathrm{Fr}=U_i^2/gR$. The predicted pinch-off depths for all the experimental conditions are tabulated in Table II. As can be seen, for the largest sphere, $D=40$ mm, the collapse of the cavity will be obstructed by the sphere itself, whereas for the smaller spheres this may not be the case, although rebound of the spheres from the bottom of the fluidization column cannot be ruled out. Note also that the simple scaling presented by Lohse *et al.*[3] does not include any effects of varying packing fraction, which will clearly influence the penetration of the sphere.

As mentioned previously, the air pressure reduction behind the falling sphere can affect the initial spray of surface particles from the corona splash. In fact, for the finer particle sizes, the corona collapses in on itself completely before the jet has emerged. This phenomenon can be seen in Fig. 8 for a 10 mm sphere impacting a bed of 65 μm particles under constant aeration yielding a packing fraction $\phi=0.54$. The influence of the air flow is most readily seen in the middle row of images at times $t=20$, 30, and 50 ms after impact. The radial collapse of the corona is met by the rapidly rising thin top jet, which is clearly more prone to disturbance than its thicker bottom, and the joint appears distorted, as seen in the last frame at 110 ms after impact. This distortion clearly affects reproducibility and is reflected in the data for maximum jet height by the much larger error bars [see Fig. 6(b)] for $\phi<0.54$. Under such circumstances, the jet height may no longer be an appropriate measure of the dynamics of the cavity collapse.

Figure 9 shows that the same general pattern of the emergence of the two-jet structure was also observed for the smaller vessel ($h_r=33$ cm) for decreasing packing fraction, although the values of ϕ required to observe this phenomenon are higher than for the larger vessel. All images shown are single frames taken at 100 ms after impact. Image (a) for the impact under no aeration ($\phi=0.62$) shows no sign of fragmentation into two jets. Image (b) for $\phi=0.59$ has begun to fragment, while in images (c) and (d) ($\phi=0.58$ and 0.57, respectively) the effect is quite profound, with distinct shoulders appearing on top of the thick bottom jet. Such a pronounced distinction was not seen for the 78 μm particles for the 10 mm sphere in the larger vessel (Fig. 4), where the packing fractions were even lower than those used here. The dependence of this phenomenon on the geometry used is not clear at this stage and may require further experimental study.

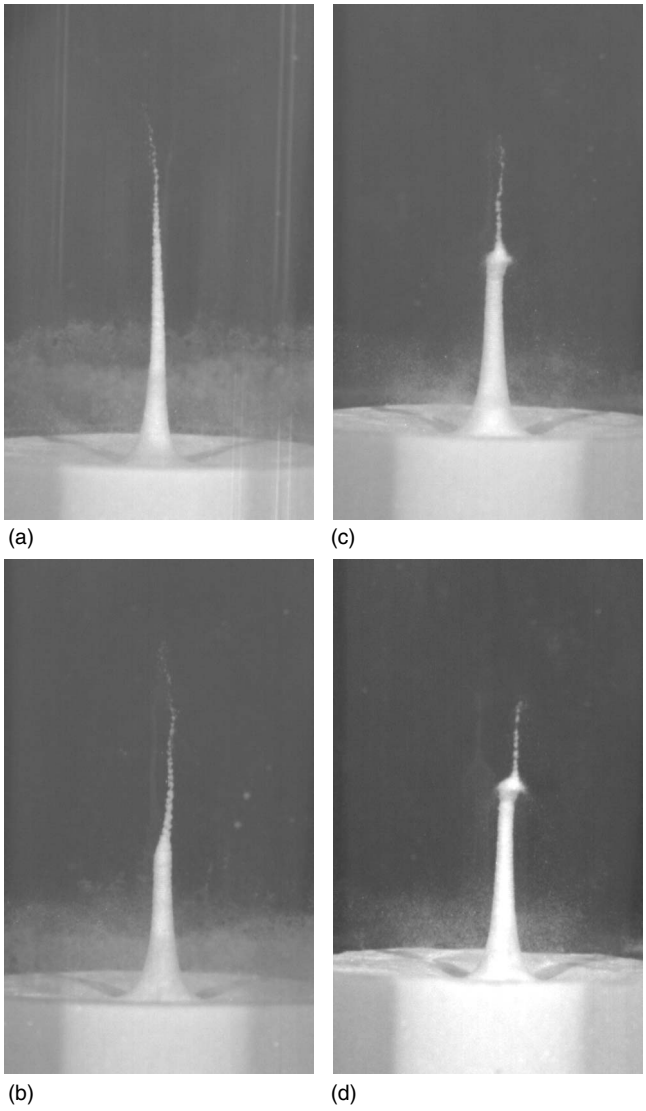

FIG. 9. Comparison of post-impact jetting under various bed packing conditions for a 10 mm sphere impacting a 7 cm deep bed (small vessel, I.D.=7 cm) of 78 μm particles from a height of 33 cm. All images are taken at 100 ms after impact. The packing fractions were (a) $\phi=0.62$, (b) $\phi=0.59$, (c) $\phi=0.58$, and (d) $\phi=0.57$.

The conditions required for the transition to a two-stage jet structure are summarized in Table III. Note that in some cases, the transition was not observed under the range of experimental conditions possible with the current equipment. The values for the large vessel clearly suggest that, for the

TABLE III. Experimental conditions for the transition to a two-stage jet structure. In some cases, no transition was seen.

Vessel I.D. (cm)	7	7	7	7	15	15	15	15
Release height, h_r (cm)	33	33	33	33	90	90	90	90
Bed height, h_b (cm)	7	7	7	7	10	10	10	10
Bead diameter, d_b (μm)	65	65	78	78	65	65	78	78
Ball diameter, D (mm)	10	20	10	20	10	20	10	20
Critical packing fraction, ϕ_c	<0.6	n/a	<0.59	n/a	0.54	<0.54	<0.53	<0.53

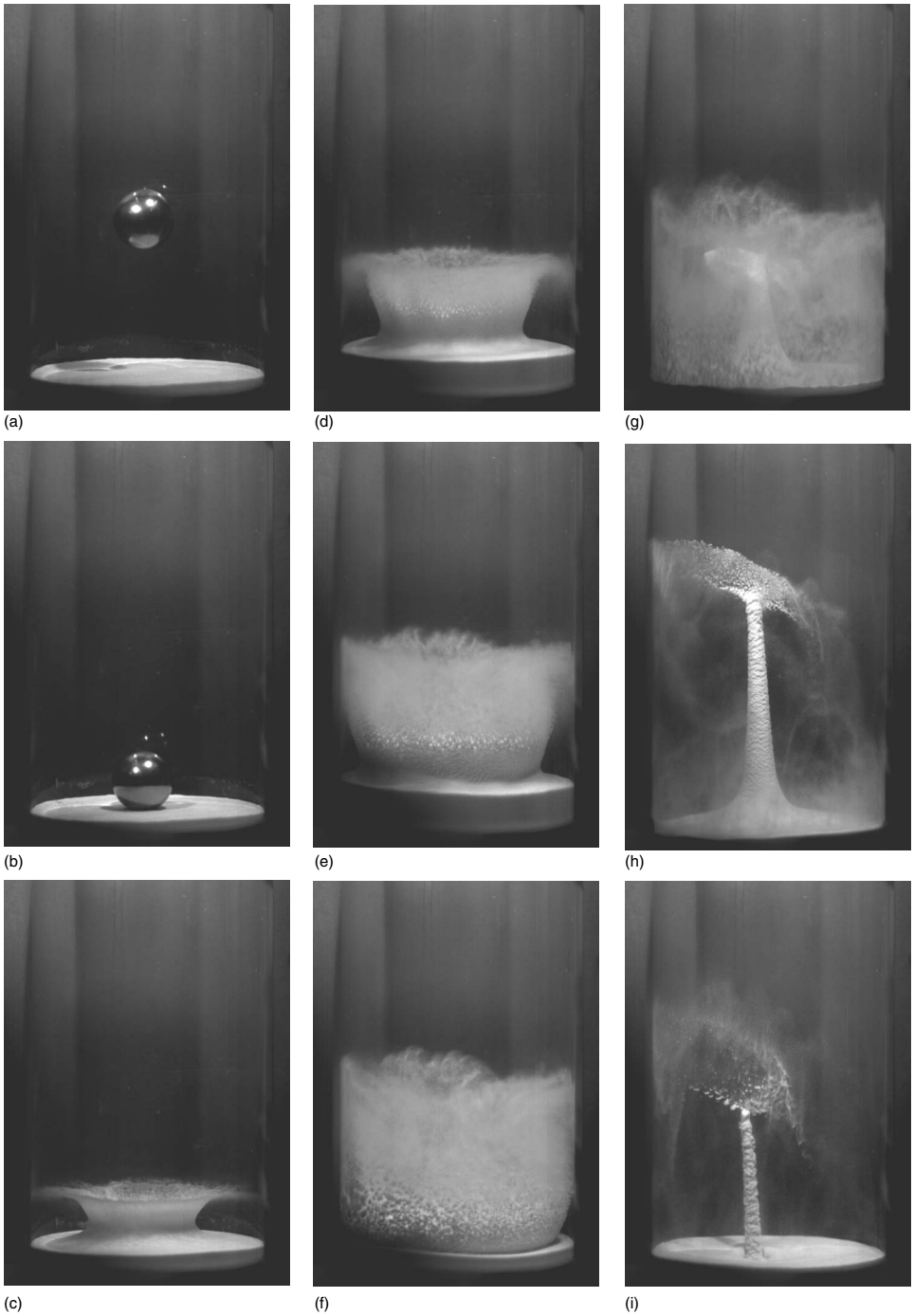

FIG. 10. Sequence of events for impact of a 40 mm sphere onto a 10 cm deep bed of 65 μm particles from a release height of 90 cm. There was no aeration during impact for these images, yielding a packing fraction, ϕ=0.57 Times from impact are −20, 0, 20, 50, 100, 150, 200, 300, and 433 ms.

range of parameters used in this study, the onset of the two-jet structure is independent of the size of the impacting sphere.

To investigate possible wall effects, some experiments were performed for a larger sphere, D=40 mm, in both the large and small vessels. Figure 10 shows the sequence of events for the impact of the 40 mm sphere onto a 10 cm deep bed (large vessel) of 65 μm particles (ϕ=0.57). The increased impact force results in a much larger corona, which expands to hit the vessel wall about 100–150 ms after impact. The resulting jet formation is somewhat distorted—a thick jet with a "sheet" of beads is clearly seen 300 ms after impact.

It is possible in this case that the collapse of the cavity will be disrupted by the sphere itself since the depth of the bed is only 2.5 times the diameter of the sphere. However, it is not possible (with the present equipment) to visualize the interaction between the sphere and the collapse of the cavity in this geometry.

Figure 11 shows the impact of the 40 mm sphere onto a 7 cm deep bed (small vessel) of 78 μm particles. In this instance, the sphere diameter is comparable to both the diameter of the vessel and the height of the bed. The corona again hits the vessel walls and rises sharply up. No jetting is seen, but a fine spray of beads emerges as the corona falls. In this instance, it is clear that the sphere prevents the usual

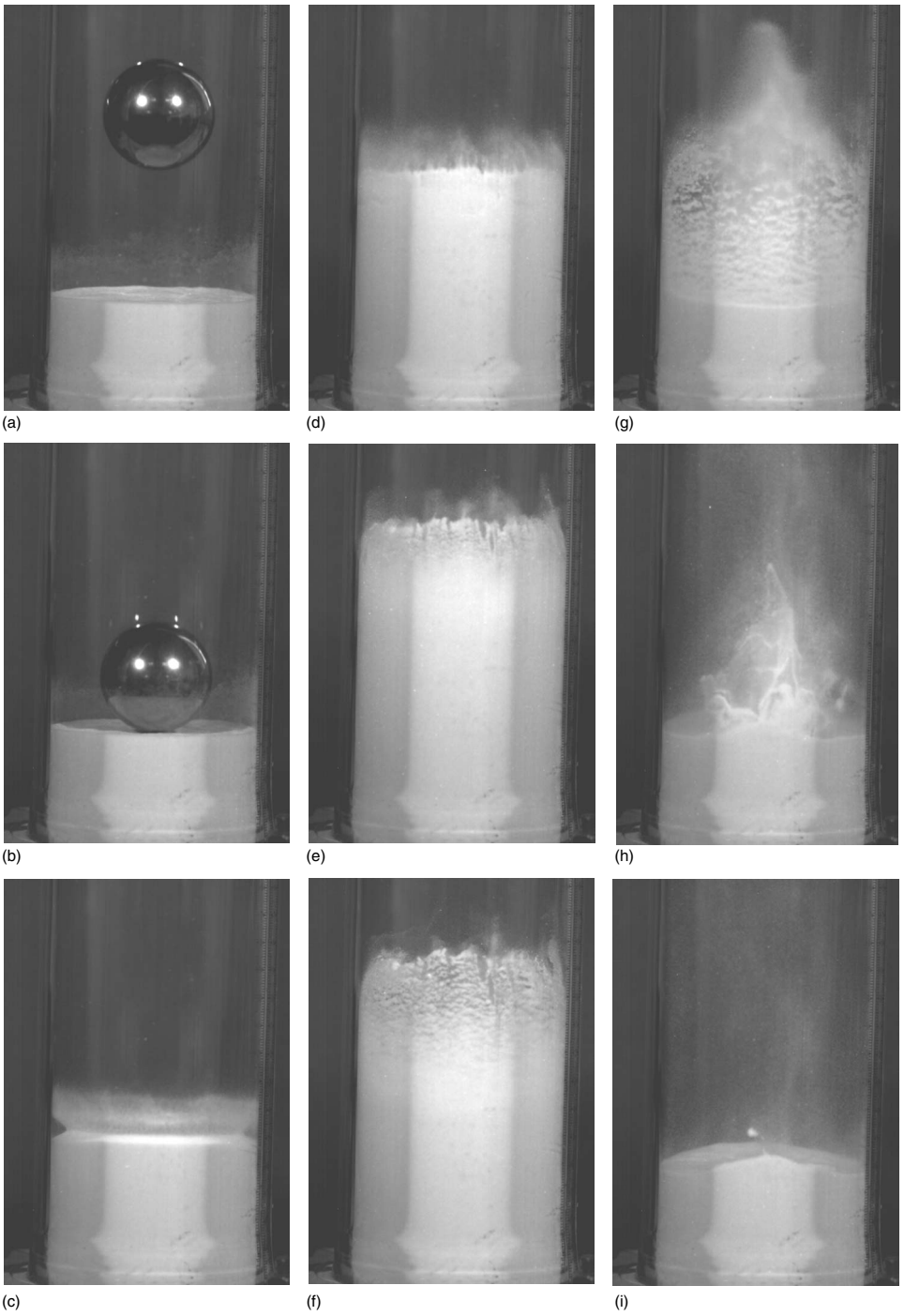

FIG. 11. Sequence of events for impact of a 40 mm sphere onto a 7 cm deep bed (small vessel, I.D.=7 cm) of 78 μm particles from a release height of 33 cm. There was no aeration during impact for these images, yielding a packing fraction, ϕ=0.62. Times from impact are −20, 0, 20, 50, 100, 150, 200, 300, and 400 ms.

cavity pinch-off and hence the emergence of a jet. The ejection of particles in this case must be between the sphere and the container walls; visualization of this would be useful to completely describe the dynamics.

IV. CONCLUSIONS

An experimental study of the phenomena following the impact of stainless steel spheres onto granular beds has been performed. The main parameter that was varied throughout this study was the level of aeration in the bed during impact, corresponding to different initial packing fractions. Under certain conditions, the granular jet emerging from the bed takes on a two-stage structure: one thin jet, which is always seen, and one thick jet, which becomes apparent only below threshold values of the packing fraction. This two-stage structure has only been reported before by Royer *et al.*[6] as a result of varying the ambient gas pressure, not the conditions in the bed. As such, it seems plausible that in their experiments, by changing the ambient pressure, they inadvertently changed the packing state in the bed. In light of this, the mechanism for the formation of the thick jet given by Royer *et al.*,[6] i.e., compression of the cavity that, in the presence of high ambient pressure, gives rise to the thick jet, may need readdressing. Aeration in the bed will inevitably interact dynamically with the cavity collapse. As such, the air flow through the bed will be channeled into the cavity and may

induce the two-stage structure at higher aeration levels. However, the extent of this effect is difficult to quantify at this stage.

The maximum jet height was found to be dependent on the packing fraction for the larger particle and sphere sizes. Experiments performed for large spheres where the diameter was comparable to the diameter of the vessels show no dependence on packing fraction, indicating that the process is highly dependent on geometry and that particle-wall interactions will affect the jet formation. This observation may also pertain to the results of Royer *et al.*[6] for their more confined geometries.

Extensions of this work might include the visualization of the interaction of the sphere and the collapsing cavity to aid the understanding of the jet formation in shallower beds.

Experiments performed with granular media are particularly useful when comparing to equivalent situations in liquids (in terms of flow geometry and material properties such as effective viscosity) with regard to topology changes (e.g., jet rupture), with a view to gaining useful insight, since the modeling is especially difficult in a continuum model near topology changes. However, the small length scales observed near break up in a liquid case will not be observed in the granular case since the length scales observed may be orders of magnitude smaller than the length scale of particles used in granular flows. As such, more experiments on granular flows comparing to an equivalent liquid case are needed to aid modeling where topological changes in the flow domain take place.

ACKNOWLEDGMENTS

The authors wish to thank the EPSRC for loan of the Photron high-speed camera for the duration of the experimental work. We also thank the reviewers for helpful comments and suggestions for improvements to the paper.

[1] A. L. Yarin, "Drop impact dynamics: Splashing, spreading, receding, bouncing," Annu. Rev. Fluid Mech. **38**, 159 (2006).
[2] S. T. Thoroddsen and A. Q. Shen, "Granular jets," Phys. Fluids **13**, 4 (2001).
[3] D. Lohse, R. Bergmann, R. Mikkelsen, C. Zeilstra, D. van der Meer, M. Versluis, K. van der Weele, M. van der Hoef, and H. Kuipers, "Impact on soft sand: Void collapse and jet formation," Phys. Rev. Lett. **93**, 198003 (2004).
[4] M. Hou, Z. Peng, R. Liu, Y. Wu, Y. Tian, K. Lu, and C. K. Chan, "Projectile impact and penetration in loose granular bed," Sci. Technol. Adv. Mater. **6**, 855 (2005).
[5] M. Hou, Z. Peng, R. Liu, K. Lu, and C. K. Chan, "Dynamics of a projectile penetrating in granular systems," Phys. Rev. E **72**, 062301 (2005).
[6] J. R. Royer, E. I. Corwin, A. Flior, M-L. Cordero, M. L. Rivers, P. J. Eng, and H. M. Jaeger, "Formation of granular jets observed by high-speed X-ray radiography," Nat. Phys. **1**, 164 (2005).
[7] S. V. Bulychev, D. V. Vyalykh, A. E. Dubinov, I. L. L'vov, S. A. Sadovoi, and V. D. Selemir, "Generating cumulative jets on the surface of granular medium," Dokl. Phys. **51**, 486 (2006).
[8] D. Geldart, "Types of gas fluidisation," Powder Technol. **7**, 285 (1973).
[9] D. Geldart, *Gas Fluidization Technology* (Wiley, New York, 1986).
[10] M. E. Möbius, "Clustering instability in a freely falling granular jet," Phys. Rev. E **74**, 051304 (2006).